Fermi National Accelerator Laboratory

FERMILAB-Conf-82/34-EXP
7180.557

# PROPERTIES OF HIGH TRANSVERSE ENERGY HADRONIC EVENTS*

B. Brown, P. Devenski, S. Gronemeyer, H. Haggerty, E. Malamud, and P. Rapp
Fermi National Accelerator Laboratory, Batavia, Illinois 60510

and

R. Abrams, H. Goldberg, C. Halliwell, F. Lopez, S. Margulies, D. McLeod, and J. Solomon
University of Illinois-Circle Campus, Chicago, Illinois 60680

and

A. Dzierba, J. Florian, R. Heinz, J. Krider, J. Martin, D. Petersen, and S. Teige
Indiana University, Bloomington, Indiana 47401

and

R. Ellsworth, R. Glasser, R. Holmes, L. Myrianthopoulos, H. Strobele, G. Yodh, and A. Zieminski
University of Maryland, College Park, Maryland 20742

and

S. Ahn and T. Watts
Rutgers University, New Brunswick, New Jersey 08903

March 1982

*Presented by Clive Halliwell at XVII Rencontre de Moriond, Les Arcs, France, March 14-26, 1982.

Operated by Universities Research Association Inc. under contract with the United States Department of Energy

# PROPERTIES OF HIGH TRANSVERSE ENERGY HADRONIC EVENTS

B. Brown, P. Devenski,[+] S. Gronemeyer, H. Haggerty, E. Malamud, P. Rapp,
FERMILAB

R. Abrams, H. Goldberg, C. Halliwell, F. Lopez, S. Margulies, D. McLeod, J. Solomon,
UNIVERSITY OF ILLINOIS (CHICAGO CIRCLE)

A. Dzierba, J. Florian, R. Heinz, J. Krider, J. Martin, D. Petersen, S. Teige,
INDIANA UNIVERSITY

R. Ellsworth,[‡] R. Glasser, R. Holmes, L. Myrianthopoulos,[x] H. Strobele, G. Yodh, A. Zieminski,[*]
UNIVERSITY OF MARYLAND

S. Ahn, T. Watts
RUTGERS UNIVERSITY

## ABSTRACT

Cross sections and event structure for events produced in pp and pA collisions with high transverse momentum are presented. The events were studied using the large acceptance Fermilab Multiparticle Spectrometer. The pp cross sections are substantially larger than predictions from the 4-jet QCD model. Production at high transverse momentum from nuclear targets increases more rapidly than the atomic mass number. The majority of the pp events are non-planar. After applying cuts to the data there is a tendency for high transverse momentum events to be more planar than ones with lower transverse momentum.



## 1. INTRODUCTION

The hadronic production of high transverse momentum (high $p_t$) secondaries is expected to result from the fundamental collision of hadronic constitutents rather than a collision between hadrons as a whole.[1] Such production may be considered as being due to the formation and subsequent fragmentation of 'jets'.[2] In this case, an understanding of single particle production will be complicated by the fact that detailed knowledge of 'jet' fragmentation is necessary. To avoid this complication, several experiments[3] have attempted to trigger on 'jets' by demanding that a large value of $p_t$ be confined to a small volume of phase space rather than to just a single particle. The drawback of this scheme is that prior knowledge of the 'jet' size is essential. Recently three large acceptance experiments, NA5 at CERN[4], E609 and E557 at Fermilab, have attempted to overcome this latter difficulty by relaxing the geometrical phase space requirement whilst retaining the necessity for a large value of $p_t$ in an event.

This report presents preliminary results from the E557 experiment. It is organized as follows; in Section 2 a brief description of the apparatus is given followed in Section 3 by the analysis procedure. In Section 4 preliminary cross sections are presented and compared to measurements from other experiments. Sections 5 and 6 include preliminary results on event structure and nuclear target cross sections respectively. Finally, conclusions are drawn in Section 7.

## 2. EXPERIMENTAL METHOD

The E557 experiment was performed using 400 GeV diffractively produced protons from the M6W beam line at Fermilab. The beam was incident on a 45cm $H_2$ target followed downstream by two interchangeable metal foils of Al, Cu or Pb.

The detection apparatus consisted of the Fermilab multiparticle spectrometer as shown in Fig. 1. Multiwire proportional chambers (34 planes of 8500 wires) and magnetostrictive spark chambers (24 planes) detected charged particles. The charged particles were identified using two multicell Cherenkov counters and their momenta were measured using a spectrometer magnet that provided a .2 GeV/c $p_t$ kick. Downstream of the tracking chambers was placed a 2.2 x 3 m highly segmented calorimeter consisting of 280 modules. The upstream section, which consisted of 126 lead-scintillator (16 r.l.) sandwiches, primarily detected and measured the energy of electromagnetic particles; the

downstream section of 154 iron-scintillator sandwiches (7.5 a.l.) measured the hadronic energy.[5] The calorimeter served as a trigger (see below) and a detector of neutral and charged particles. This was achieved by splitting the output of each module into two, one half being used in the trigger electronics and the other going to an ADC whose output was used in off-line analyses.

The geometrical acceptance of the calorimeter was approximately $2\pi$ in azimuth over the polar angle range $50° < \theta < 130°$ as measured in the proton-proton centre-of-mass frame. This corresponded approximately to a rapidity, y, range of 1.5 centered at $y^* = 0$.

The apparatus was triggered in two ways. Firstly, an inelastic collision was detected by demanding either that an incident proton had lost enough energy to miss a small counter placed on the beam line downstream of the magnet or that a large pulse height was present in a counter placed immediately downstream of the target. This constituted the 'interacting beam trigger' (in later analysis it was determined that this trigger was sensitive to approximately 90% of the total inelastic cross section). The second trigger consisted of the 'interacting beam' trigger with an additional requirement that a certain amount of transverse energy was present in the calorimeter (hereafter designated '$E_t$').

$E_t$ for each module was formed by weighting its output by the sine of its angle formed from the target with respect to the incident beam direction. Then, $E_t$ sums for several different configurations of calorimeter modules were formed. Data from three are presented in this report. The configurations used were full azimuthal acceptance ('$2\pi$'); two $2\pi/5$ apertures diametrically opposed to each other ('$4\pi/5$'); small aperture ('$\pi/5$'). They had approximate acceptances of 8.2, 2.9 and 0.75 steradians in the proton-proton centre-of-mass frame.

To determine the absolute $E_t$ scale the calorimeter was calibrated twice, before and after the 18-day data run, by directing a 20 GeV/c beam of electrons and hadrons into each module. The total uncertainty $E_t$ is estimated from the calibration and other sources to be $\sigma_{E_t}/E_t = \pm 5\%$.

For this report only vertex data (for hydrogen-nuclear target separation) and calorimeter data have been used. No data are presented that depended on the spectrometer or Cherenkov counters. Consequently no correction for the magnetic field $p_t$ kick has been attempted at this stage.



## 3. ANALYSIS

Corrections were applied to the pulse height sums in the $E_t$ determination. For example, the response of the lead-scintillator section of the calorimeter was different (by approximately 17% at 40 GeV) for hadrons and photons of the same energy. Consequently, knowledge of the type of particle hitting the calorimeter was necessary for a correct analysis. This was obtained by comparing the responses from the lead-scintillator and iron-scintillator sections of the calorimeter. Another correction was needed in the calculation of the position that particle hit the calorimeter. Assuming that it always hit the centre of a module would have introduced errors in the $E_t$ calculation. This was overcome by forming spatial 'clusters' of energy. The weighted centre of these clusters produced a more accurate estimate than the modules centres. The extent of these 'clusters' was compared to predictions from a shower production simulation.[6] By this method it was possible to determine whether, for example, adjacent fired modules were caused by one or two particles. The results of forming these 'clusters', is shown in Fig. 2 where the invariant cross section for 'cluster' production is compared to the sum (solid line) of charged[7] (dashed line and triangles) and $\pi^0$[8] single particle measurements at 90 degrees. To make the comparison more meaningful the calorimeter resolution[5] has been estimated and the result is the long-dash curve. The reasonable agreement between the single particle and the 'cluster' measurements lends credence to the idea that 'clusters' do indeed correspond to individual particles. This comparison does not take into account such effects as $K_L^0$ and neutron production, $p_t$ kick of the magnet etc.

The cross sections changed by less than 20% when pulse heights were used rather than 'clusters'. However, the 'cluster' formation technique was invaluable for the event structure analysis.

## 4. CROSS SECTIONS

Cross sections for events with $E_t$ values up to 10 GeV were measured using the 'interacting beam' trigger. Results using the full azimuthal ( $2\pi$) acceptance of the calorimeter are shown in Fig. 3. With them are presented cross sections obtained by imposing ever increasing $E_t$ thresholds. By doing this it was possible to study events with $E_t$ values of up to 24 GeV (note that the kinematic limit is 27.4 GeV). The effect of the $E_t$ threshold is clearly visible in Fig. 3. Note the excellent agreement between data obtained with 4, 6 and 9 GeV thresholds and 'interacting beam' data. This is evidence that the calorimeter triggering logic performed correctly.

The best estimate for the production cross section is obtained by drawing an envelope through the highest points. This envelope approximates to the form $d\sigma/dE_t = e^{-.85E_t}$ for $E_t$ values above 10 GeV. This is shown in Fig. 4 along with two sets of cross sections obtained using smaller fractions of the calorimeter; the rapidity acceptance for these latter data was approximately 1.5 units as in the $2\pi$ case.

Cross sections for smaller acceptance triggers can be obtained by an alternative method using the data from the $2\pi$ trigger alone. For each event the $E_t$ within a small acceptance was calculated and the probability of such an occurence was recorded. A typical example is shown in Fig. 5 where an acceptance of $\Delta\phi = \pi$ was used (the rapidity range was 1.5 as before). As in the $2\pi$ case the envelope of the highest points is the best estimate of the cross section. Parameterizing the data above 4 GeV results in $d\sigma/dE_t \sim e^{-1.4E_t}$. This procedure was repeated for acceptances of $\pi/2$, $\pi/4$, $\pi/8$ and $\pi/16$ with the resulting cross section parameterizations having slopes of -1.9, -2.4, -2.7 and -3.2 respectively. The error on these slopes is estimated at ±0.2.

The software method confirms the trend observed using small acceptance hardware triggers, that is, the increasing $E_t$ dependence of cross sections measured over decreasing acceptances. This method has the added advantage of being able to determine cross sections for arbitrary sized acceptances from a single data set. This could be useful when testing theoretical models for the production of these high $E_t$ events.

The $2\pi$ cross sections from E557 are substantially larger than the corresponding NA5 data[4]; they also have a weaker $E_t$ dependence. The different incident energies (400 GeV for E557, 300 GeV for NA5) make a direct comparison difficult. In an attempt to take this into account the cross sections were considered to depend on the variable $x_t = E_t/\sqrt{s}$, where s is the total centre-of-mass energy squared, rather than $E_t$. Doing this results in both data sets having similar slopes as seen from Fig. 6. Similar conclusions are reached when the NA5 data using smaller acceptance hardware triggers ($\pi$ and $\pi/2$) are compared to E557 data obtained by the software method. No conclusions based on the normalization difference between the two experiments should be drawn as the $E_t$ scales in both experiments have ±5% errors. The two experiments also cover slightly different regions of phase space.

Finally, the ratio of the $\pi/4$ acceptance invariant cross sections (obtained by the software method) compared to the single particle data shown in Fig. 2 was calculated. It increases from ~20 at 3 GeV to ~100 at 6 GeV confirming an effect that had already been observed in a previous experiment[9].



## 5. EVENT STRUCTURE

Event structure was studied employing the variable, planarity (P), as used by the NA5 group[4]. This was calculated in the transverse plane of the event. In this projection an event axis was found and the $p_t$ vector for each module was decomposed into components parallel and transverse to this axis. Denoting the sum of the squared components along and transverse to the principal axis as A and B, then planarity is defined as $P = (A-B)/(A+B)$. P was then minimized. For pencil-like back-to-back jets, P approaches 1 while for isotropic events it approaches 0. Fig. 7(a) shows the observed planarity distributions for events with $E_t > 14$ GeV for the $2\pi$ data sample. It is clear that the majority of the events are non-planar. The fraction of high planarity events ($P > 0.7$) stays constant with $E_t$. Fig. 7(b) shows the variation of the mean planarity with $E_t$. For $E_t < 6$ GeV the planarity rises because of the very low multiplicity in the calorimeter. Above $E_t = 6$ GeV the planarity indicates a mostly isotropic distribution of secondaries unaffected by increasing $E_t$.

To study event structure in a more detailed way 'clusters' rather than pulse heights were used. Even though 'clusters' were used, the determination of where a particle hit the calorimeter was still seriously effected by the calorimeter granularity. The granularity effect was more apparent in the polar angle calculation than the azimuthal angle. Consequently, only detailed event structure in the plane transverse to the incident beam direction will be discussed here.

To reduce the granularity effect, calorimeter 'sectors' were used rather than energy 'clusters'. To do this the calorimeter was divided into 12 equal azimuthal sectors and the $E_t$ from the 'clusters' within each sector was calculated. A typical $E_t$ flow with respect to the centre of the sector with the maximum $E_t$, the 'maximum sector', is shown in Fig. 8. The dominant structure is an enhancement in the 90 to 180 degree region (the 'away' side). This increases with total $E_t$ and with the fraction of the total $E_t$ in the 'maximum sector' as shown in Fig. 9. A similar effect has previously been seen in single particle data[10].

To see if the event structure depended on the total $E_t$, the data of Fig. 9 were normalized and the results are shown in Fig. 10. Events with small and large total $E_t$ values are similar only when there is a small fraction of the total $E_t$ in the 'maximum sector'. This is not too surprising as this constraint imposes isotropy on the event. When a larger fraction of the

total $E_t$ is in the 'maximum sector', the higher $E_t$ data show a greater enhancement on the 'away side' indicating an increase in clustering. It is important to note that the amount of clustering present in the data is far less than that expected from 4-jet events[11].

In an attempt to see how much of the 'away side' enhancement is due to $p_t$ conservation, the directions of the 'clusters' in an event were randomized in the transverse plane, (their polar directions were preserved). Tracks within the 'maximum sector' were not included. This randomization was repeated until the magnitude of the final $p_t$ vector sum was within 10% of the original sum. The final direction of the vector sum had to be within 30° of the original. This randomization scheme preserves the total $E_t$ in an event. The results, shown in Fig. 9, indicate that the difference between the original and randomized $E_t$ flows grows with total $E_t$, showing once again, an increase in clustering at higher $E_t$ values. However, it can be seen that the main contribution to the event structure appears to be $p_t$ conservation.

## 6. NUCLEAR TARGET CROSS SECTIONS

Typical vertex distributions are shown in Fig. 11(a) and 11(b) for 'interacting beam' and $2\pi$ data ($E_t > 15$ GeV). The dramatic growth of the nuclear targets signal compared to $H_2$ indicates that the dependence of the $2\pi$ cross section on atomic mass number is stronger than that for inelastic cross sections.

Events originating from the two nuclear foils were separated from the hydrogen events by performing a vertex position fit (see Fig. 11(c)). The simultaneous data collection from different targets eliminated many systematic errors. From the production rate, cross sections were calculated. A typical sample of the data is shown in Fig. 12. It is clear that the data are consistant with the parameterization $d\sigma/dE_t \sim A^{\alpha(E_t)}$ when the hydrogen data are not included. The hydrogen data have not been corrected for the small acceptance difference due to the downstream positioning of the nuclear targets.

The variation of $\alpha$ as a function of $E_t$ for the full azimuthal acceptance trigger is shown in Fig. 13(a). $\alpha$ increases from ~2/3 at low $E_t$, becomes 1 at $E_t$ = 10 GeV rising finally to ~1.25 at 15 GeV. A similar effect is also seen for the smaller acceptance trigger ($\pi/5$) (see Fig. 13(b)). This trend for $\alpha$ to exceed unity has been seen previously in single particle production[7] and small aperture 'jet' experimentes.[12] The explanations for such behavior are numerous and varied[13].



## 7. CONCLUSIONS

The production of events with large values of transverse energy (50 to 80% of the incident energy as measured in the centre-of-mass frame) is far more frequent than that expected from QCD 4-jet predictions. This phenomenon appears to persist even at $\sqrt{s}$ = 540 GeV[14] where substantial cross sections for $E_t$ = 100 GeV have been measured. The small amount of 'jet' production is confirmed by the fact that the majority of events are not planar. It is difficult to estimate the exact fraction of events that possess 'jet-like' qualities but it appears to be less than 5% of the total data sample for high $E_t$ events.

A recent QCD approach[15], which includes the effects of gluon bremsstrahlung, appears to be successful in reproducing the large acceptance data from NA5. It will be interesting to see if it can also predict the dependence of the cross section on acceptance and reproduce the event structure as measured in this experiment.

As mentioned earlier, there is no consensus on understanding the nuclear target data.

ACKNOWLEDGEMENTS

We would like to express our appreciation to the Multiparticle Spectrometer Group headed by Dan Green for their invaluable help during the preparation of E557. We also acknowledge the contribution of B. Hanna during the early stages of the experiment. One of us (C. Halliwell) would like to thank Tran Thanh Van and his co-workers for such an enjoyable conference. Finally, we would like to thank Janet Harden who worked so hard in typing this document in time for publication.

This work was supported in part by the U.S. Department of Energy and the National Science Foundation.



REFERENCES

Permanent Address:

+ Higher Institute for Chemistry and Technology, Sofia, Bulgaria.

• Institute for H.E.P. Heidelberg, Fed. Rep. of Germany.

x Dept. of Radiology, University of Chicago.

‡ George-Mason University, Fairfax, Virginia.

* On leave of absence from the University of Warsaw, Poland.

1. Many excellent reviews have been written on high $p_t$ production. Some recent ones are.....P. Darriulat, Ann Rev. Nucl. Part Sci, 30, 159 (1980); M. A. McCubbin, Rutherford Lab preprint, RL-81-041 (1981); Wm. M. Geist, CERN preprint CERN/EP 81-79 (1981)

2. R. D. Field and R. P. Feynman, Nucl. Phys. B136, 1 (1978)

3. (A) V. Cook et al., Nucl. Phys., B186, 219 (1981),
(B) C. Bromberg et al., Phys. Rev. Lett., 43, 565 (1979)
(C) W. Selove, Proceedings of the 14th Rencontre de Moriond, Vol. 1 (1979).

4. "A Study of Deep Inelastic Hadron-Hadron Collisions with a Large Acceptance Calorimeter Trigger", C. De Marzo et al., M.P.I. preprint, submitted to Physics Letters (1982).

5. P. Rapp et al., Nucl. Inst. and Meth. 188, 285 (1981).

6. M. Della Negra Lapp Preprint Exp-07 (1980).

7. D. Antreasyan et al., Phys. Rev. D19, 764 (1979).

8. C. Kourkoumelis et al., Zeit Fur. Phys. C5, 95 (1980).

9. C. Bromberg et al., Nucl. Phys. B171, 1 (1980).

10. M. G. Albrow et al., Nucl. Phys. B145, 305 (1978).

11. A simulation containing QCD cross-sections and jet fragmentation was used. No scale breaking in the structure functions was included. None of the conclusions drawn in this report are sensitive to the specific details of the model.

12. C. Bromberg et al., Phys. Rev. Lett. 42, 1202 (1979).
C. Bromberg et al., Nucl. Phys. B171, 38 (1980).

13. One of the most recent hadron-nucleus compliations is in Fermilab preprint CONF-82/29 - THY/EXP (1982).

14. A. Kernan, UA1 talk at Topical conference on forward $\bar{p}p$ collider physics, Madison (1981).

15. G. C. Fox and R. L. Kelly, LBL-CALTECH preprint, LBL-13985, CALT-68-890 (1982).



## FIGURE CAPTIONS

Fig. 1: The Fermilab M6W Multiparticle Spectrometer. The vertical lines depict tracking chambers. The dotted line in the calorimeter signifies the hole through which small angle secondaries pass.

Fig. 2: A comparison between single-particle production (solid line) with calorimeter resolution folded in (long dashed curve), and 'cluster' formation in the calorimeter (dots).

Fig. 3: Preliminary cross sections for multiparticle production resulting in a total transverse energy of $E_t$ measured over an acceptance of 8.25sr centered approximately at $y^* = 0$. The different symbols refer to different $E_t$ thresholds. The error on the $E_t$ scale is ±5%.

Fig. 4: Comparison of preliminary cross sections obtained with large ($2\pi$), medium ($2 \times 2\pi/5$) and small ($\pi/5$) azimuthal acceptances. The $E_t$ dependence of the three data sets is indicated. The error on the $E_t$ scale is ±5%.

Fig. 5: Cross sections for $\pi$ acceptance produced from the large acceptance ($2\pi$) data using software cuts. The different symbols refer to different $E_t$ ranges. In the interest of clarity, error bars have been omitted. Typical errors on the points at the highest $E_t$ values in each $E_t$ range are ~30%. The error on the $E_t$ scale is ±5%.

Fig. 6: Comparison of E557 and NA5 data. The NA5 data at 300 GeV has been 'scaled' assuming it is a function of $E_t/\sqrt{s}$ rather than $E_t$. Also shown is a 4-jet QCD calculation (ref. 4).

Fig. 7: (a) Planarity distribution for $2\pi$ azimuthal acceptance data with $E_t >$ 14 GeV. (b) Mean planarity of the $2\pi$ azimuthal acceptance data as a function of $E_t$.

Fig. 8: A Typical $E_t$ flow using 30° sectors.

Fig. 9: $E_t$ flow in sectors as a function of azimuthal angle measured with respect to maximum $E_t$ flow direction (histogram). The horizontal and the vertical scales are the same as those shown in Fig. 8. The dots show similar results after randomizing the 'clusters' azimuthal directions (see text). The data is shown as a function of the total $E_t$ and as a function of the fraction of the total $E_t$ in the 'maximum sector' (see text). Only sectors with greater than 10% of the total $E_t$ contribute to the plot.

Fig. 10: Normalized $E_t$ flows using the data similar to that shown in Fig. 9. In this case, only sectors with greater than 5% of the total $E_t$ contribute. The three sets of data are for $E_t$ values of 3 to 7(Δ), 9 to 13 (●) and 17 to 21 GeV (○). Statistical errors only are shown. The figures (a) (b) and (c) refer to different fractions of $E_t$ in the 'maximum sector'. These fractions are; between .1 and .2, .2 and .3, .3 and .4 respectively.

**Fig.** 11: Distribution of the production vertex coordinate along the incident beam direction. (a) 'interacting beam data. The upstream $H_2$ target window is clearly visible. The two sharp black spikes are due to the nuclear targets. (b) $2\pi$ acceptance data ($E_t > 15$ GeV). (c) Enlargement of nuclear target region for $2\pi$ data. The curve superimposed on the data (histogram) is a fit of 4 gaussians (2 per peak) + constant background.

**Fig.** 12: Cross sections as a function of atomic mass number. The lines are drawn to guide the eye.

**Fig.** 13: $\alpha$ as a function of $E_t$ for (a) $2\pi$ data and (b) smaller acceptance data.



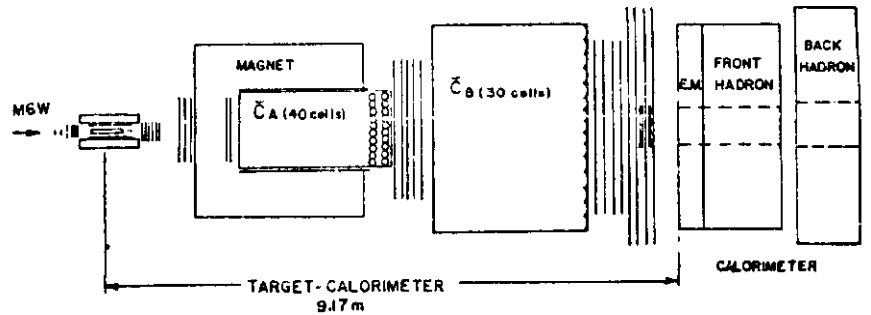


**Fig.** 1

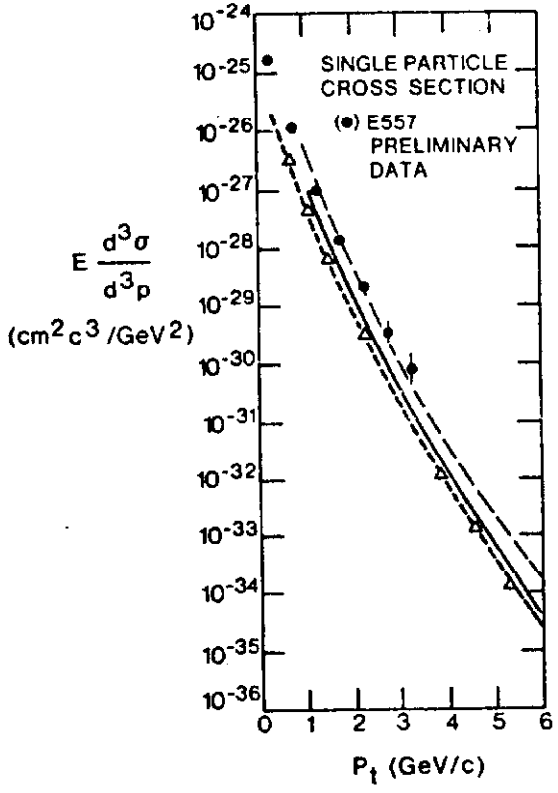
SINGLE PARTICLE
CROSS SECTION
(●) E557
PRELIMINARY
DATA
$E \frac{d^3\sigma}{d^3p}$
$(cm^2 c^3 / GeV^2)$
$P_t$ (GeV/c)

Fig. 2



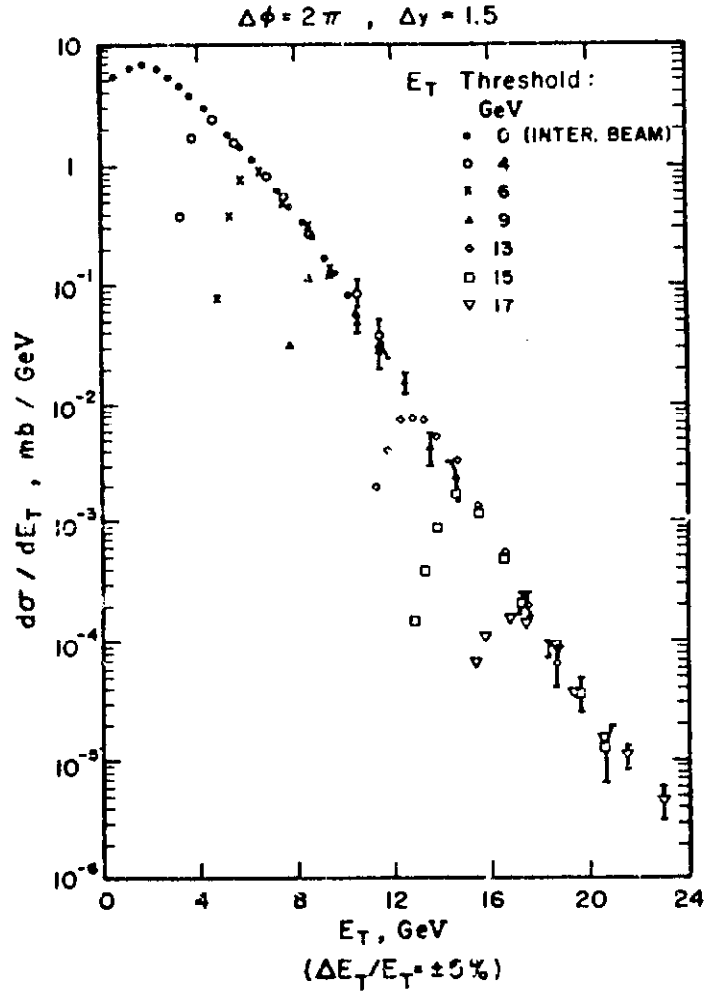
$\Delta\phi = 2\pi$ , $\Delta y = 1.5$
$E_T$ Threshold :
GeV
0 (INTER. BEAM)
4
6
9
13
15
17
$d\sigma / dE_T$ , mb / GeV
$E_T$ , GeV
$(\Delta E_T / E_T = \pm 5\%)$

Fig. 3

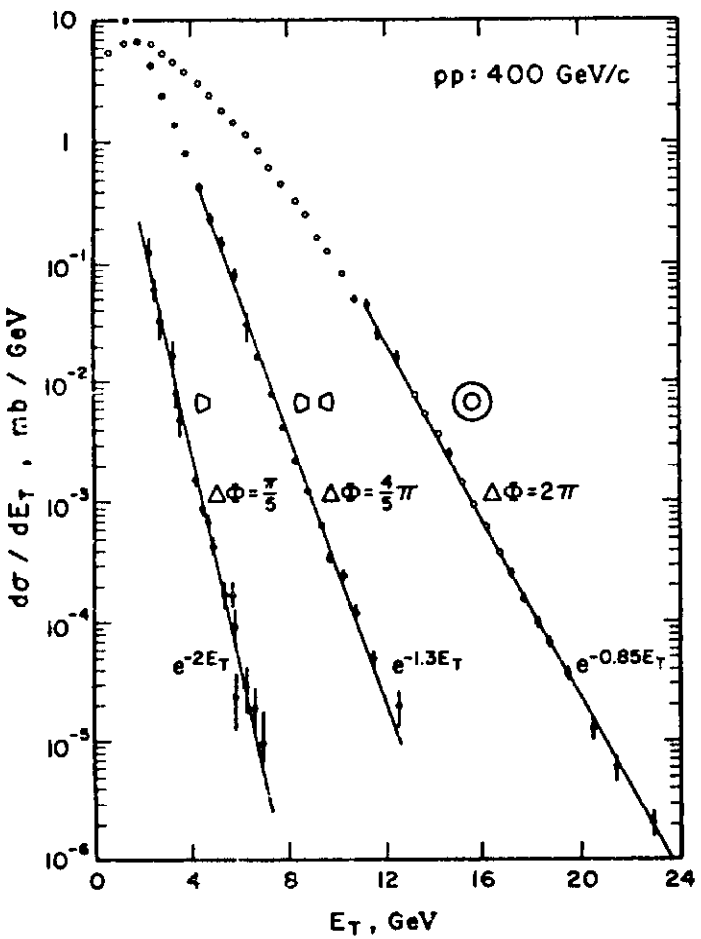
pp: 400 GeV/c
ΔΦ=π/5
ΔΦ=4/5π
ΔΦ=2π
e^-2E_T
e^-1.3E_T
e^-0.85E_T
dσ / dE_T , mb / GeV
E_T , GeV

Fig. 4



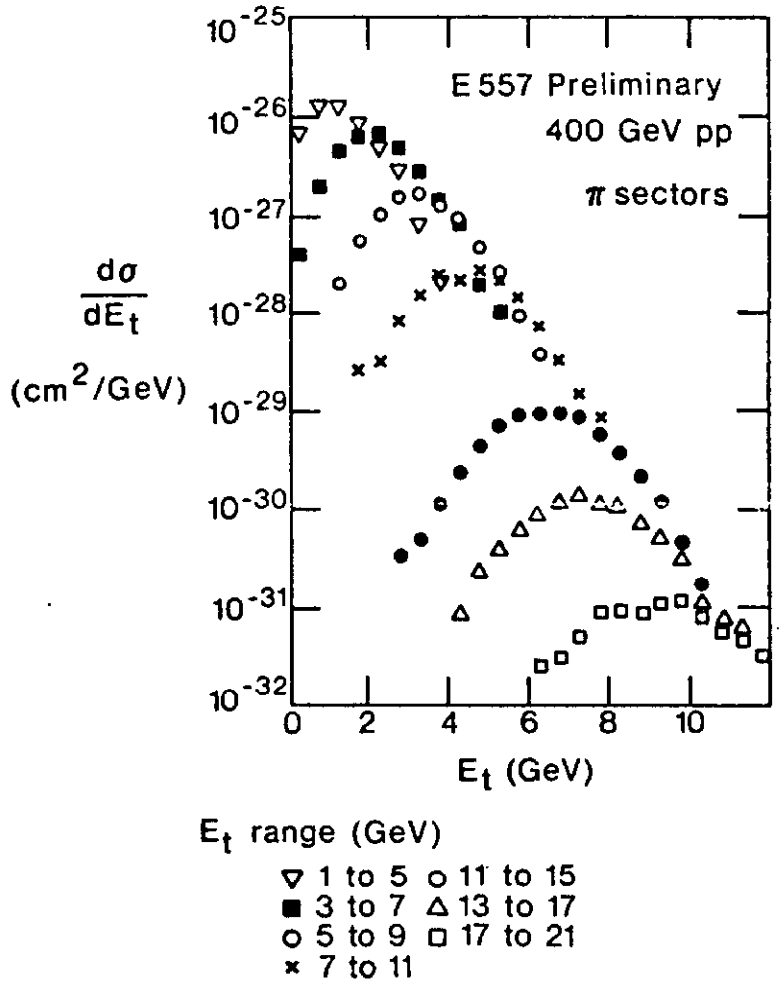
E 557 Preliminary
400 GeV pp
π sectors
dσ/dE_t
(cm²/GeV)
E_t (GeV)
E_t range (GeV)
▽ 1 to 5
■ 3 to 7
○ 5 to 9
× 7 to 11
○ 11 to 15
△ 13 to 17
□ 17 to 21

Fig. 5

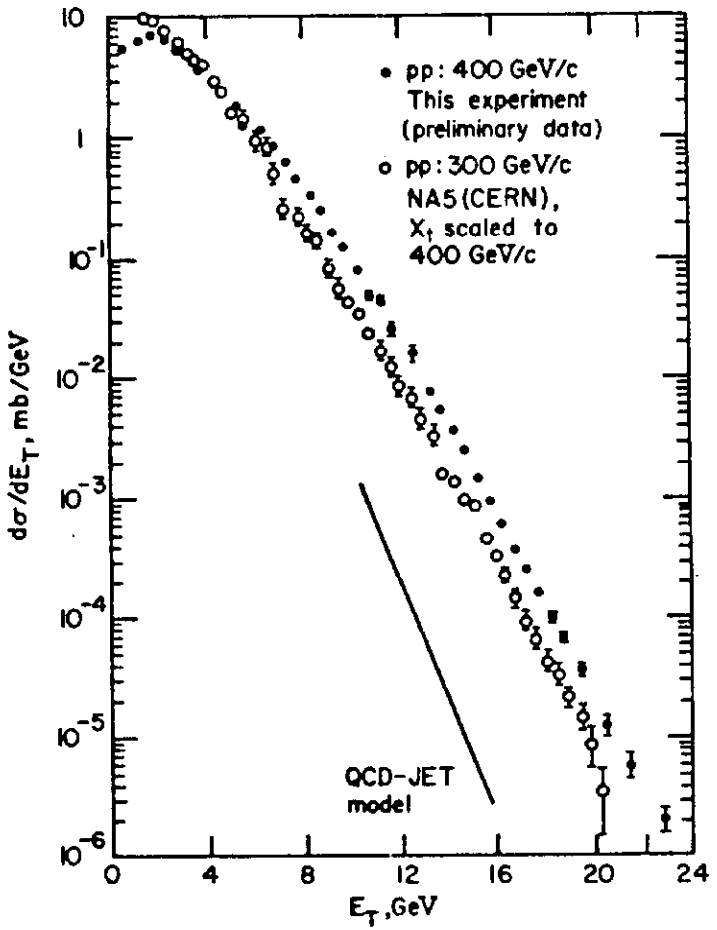
• pp: 400 GeV/c
This experiment
(preliminary data)
o pp: 300 GeV/c
NA5 (CERN),
$X_t$ scaled to
400 GeV/c
QCD-JET
model
$d\sigma/dE_T$, mb/GeV
$E_T$, GeV

Fig. 6



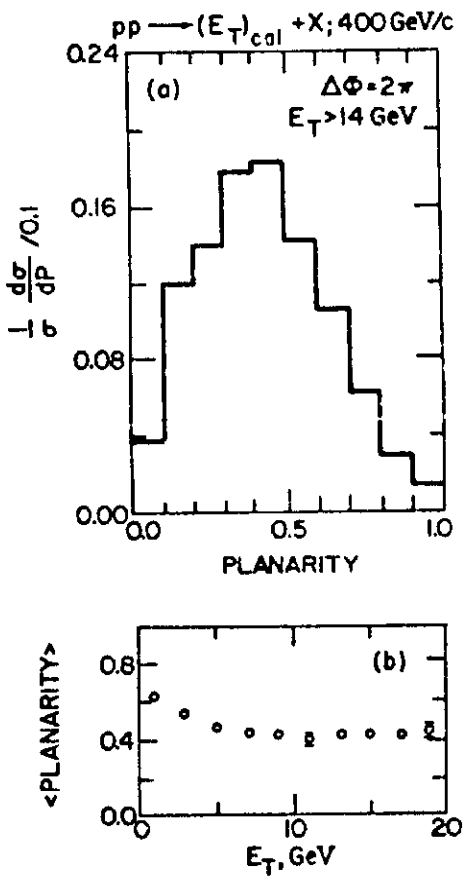
$pp \longrightarrow (E_T)_{cal} + X$; 400 GeV/c
(a)
$\Delta\Phi = 2\pi$
$E_T > 14$ GeV
$\frac{1}{\sigma}\frac{d\sigma}{dP}/0.1$
PLANARITY
(b)
<PLANARITY>
$E_T$, GeV

Fig. 7

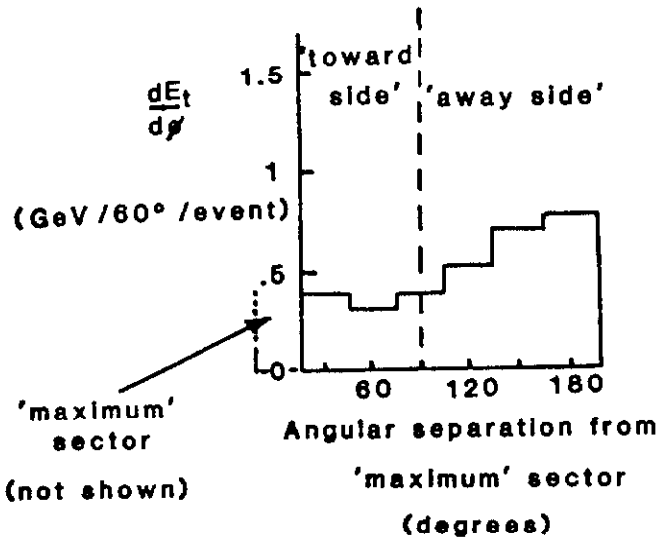
dE_t/dφ
(GeV /60° /event)
1.5
1
.5
0
'toward side'
'away side'
60
120
180
'maximum' sector
(not shown)
Angular separation from 'maximum' sector (degrees)

Fig. 8



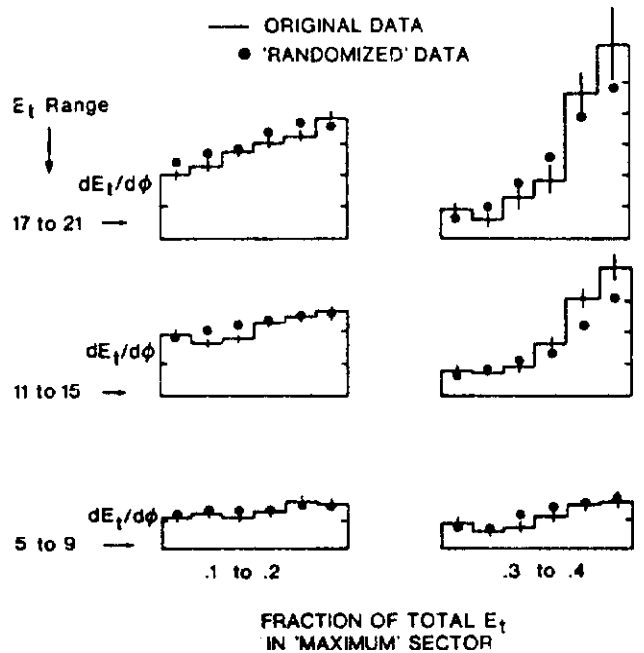
ORIGINAL DATA
'RANDOMIZED' DATA
E_t Range
dE_t/dφ
17 to 21
11 to 15
5 to 9
.1 to .2
.3 to .4
FRACTION OF TOTAL E_t IN 'MAXIMUM' SECTOR

Fig. 9

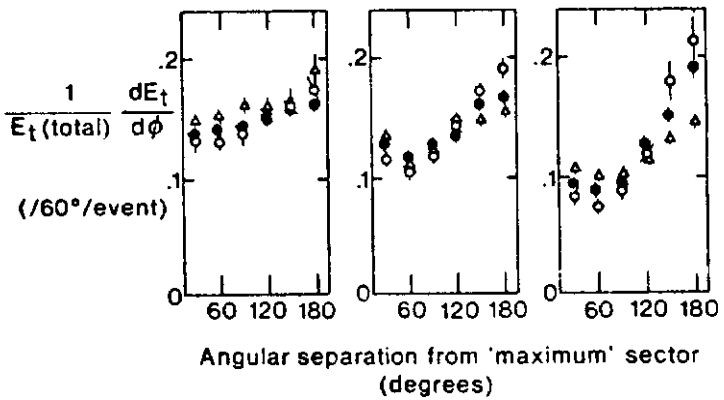
1 / E_t(total) dE_t/dφ
(/60°/event)
.2
.1
0
60 120 180
Angular separation from 'maximum' sector
(degrees)

Fig. 10



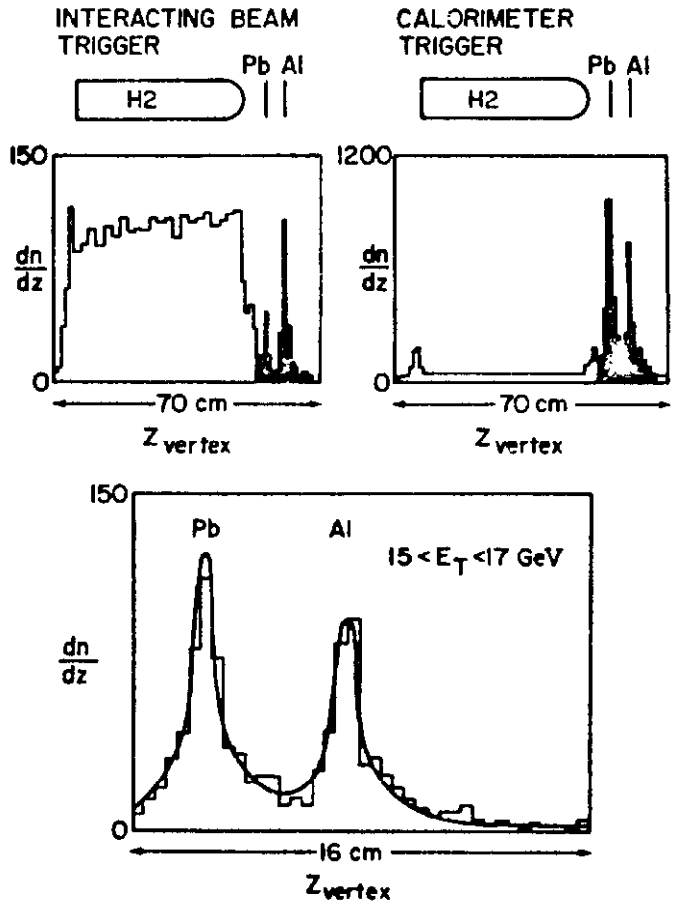
INTERACTING BEAM
TRIGGER
Pb Al
H2
150
dn/dz
0
70 cm
Z vertex
CALORIMETER
TRIGGER
Pb Al
H2
1200
dn/dz
0
70 cm
Z vertex
150
Pb
Al
15 < E_T < 17 GeV
dn/dz
0
16 cm
Z vertex

Fig. 11

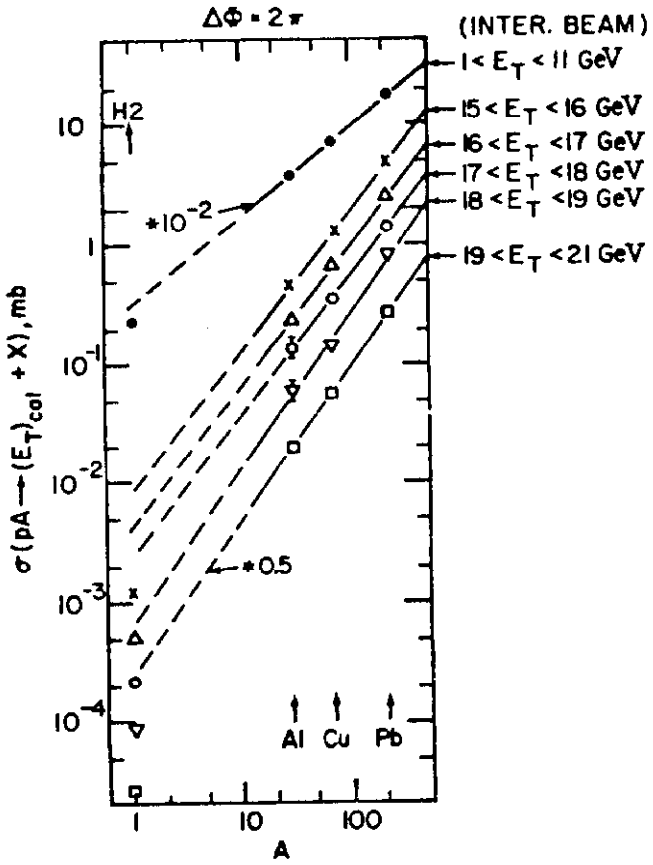
ΔΦ = 2π
(INTER. BEAM)
1 < E_T < 11 GeV
15 < E_T < 16 GeV
16 < E_T < 17 GeV
17 < E_T < 18 GeV
18 < E_T < 19 GeV
19 < E_T < 21 GeV
H2
*10^-2
*0.5
Al Cu Pb
σ(pA → (E_T)_cal + X), mb
A

Fig. 12



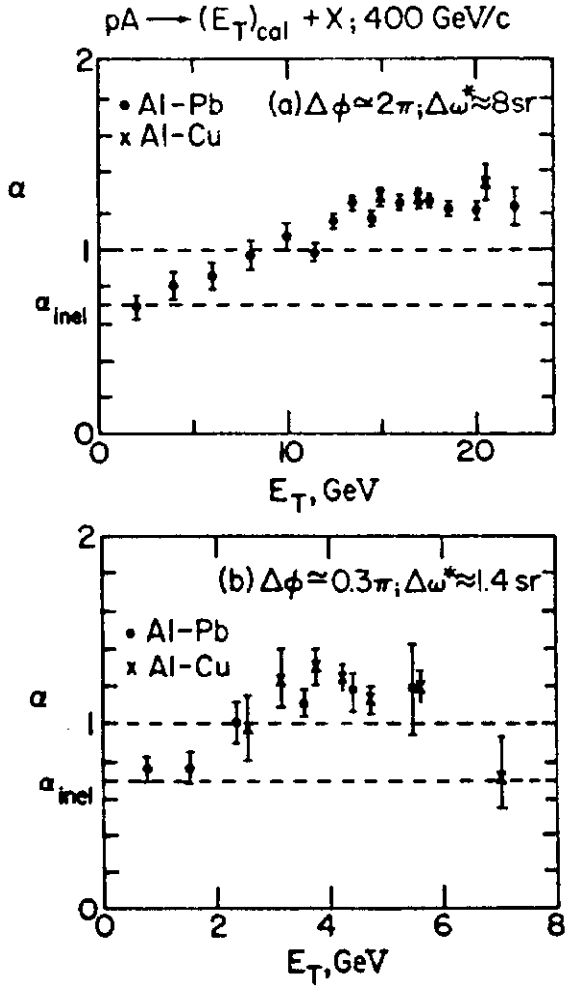
pA → (E_T)_cal + X; 400 GeV/c
• Al-Pb
x Al-Cu
(a) Δφ≃2π; Δω*≈8sr
α
α_inel
E_T, GeV
(b) Δφ≃0.3π; Δω*≈1.4 sr
• Al-Pb
x Al-Cu
α
α_inel
E_T, GeV

Fig. 13